pp 1083–1102.
doi:10.1017/aer.2021.1

Parameter optimisation of a carrier-based UAV drawbar based on strain fatigue analysis

H. Chen, **X. Fang**, **Z. Zhang and X. Xie**
College of Aerospace Engineering
Nanjing University of Aeronautics and Astronautics
Nanjing
Jiangsu
China

H. Nie and X. Wei
hnie@nuaa.edu.cn
College of Aerospace Engineering
Nanjing University of Aeronautics and Astronautics
Nanjing
Jiangsu
China
and
State Key Laboratory of Mechanics and Control of Mechanical Structures
Nanjing
Jiangsu
China

ABSTRACT

Carrier-based unmanned aerial aircraft (UAV) structure is subjected to severe tensile load during takeoff, especially the drawbar, which affects its fatigue performance and structural safety. However, the complex structural features pose great challenges for the engineering design. Considering this situation, a structural design, fatigue analysis, and parameters optimisation joint working platform are urgently needed to solve this problem. In this study, numerical analysis of strain fatigue is carried out based on the laboratory fatigue failure of the carrier-based aircraft drawbar. Taking the sensitivity of drawbar parameters to stress and life into account and optimum design of drawbar with fatigue life as a target using the parametric method, this study also includes cutting-edge parameters of milling cutters, structural details of the drawbar and so on. Then an experimental design is applied using the Latin hypercube sampling method, and a surrogate model based on RBF neural network is established. Lastly, a multi-island genetic algorithm is introduced for optimisation. The results show that the error between the obtained optimal solution and simulation is 0.26%, while the optimised stress level is reduced by 15.7%, and the life of the drawbar is increased by 122%.

Received 18 June 2020; revised 3 January 2021; accepted 6 January 2021.

Keywords: carrier-based UAV; strain fatigue; surrogate model; structural optimisation

NOMENCLATURE

b	fatigue strength exponent
Beta	cutting edge angle of slotted feed knife
c	fatigue ductility exponent
d	dimension of the design space
D_1	the distance between the axis of the drawbar body and center of groove outline cutter
D_2	the distance between the axis of drawbar head and center of groove outline cutter
D_3	the distance between the axis of the drawbar head and groove outline
D_4	the distance between the axis of the drawbar head and center of groove edge
D_5	height of groove
D_6	the distance between the axis of the drawbar head and gradient starting point
D_7	the distance between the axis of the drawbar head and gradient ending point
D_8	the initial thickness of web
E	elastic modulus
K′	cyclic strength coefficient
l_i	lower limit on the dimension
σ_f'	fatigue strength coefficient
σ_{m}	mean stress
ε_f'	fatigue ductility coefficient
$\varepsilon_{\mathrm{ea}}$	elastic strain
$\varepsilon_{\mathrm{pa}}$	plastic strain
ε_{a}	total strain
L	life repeats of the structure
me	elastic poisson's ratio
mp	plastic poisson's ratio
n	number of sample points
ϕ	basis function
λ_i	coefficient of the ith basis function
n′	cyclic strain hardening exponent
N	life repeats of the bar
Nc	cut-off
$N_{x_i'}$	percentage form of the model coefficient
R1	cutting edge radius of groove outline
R2	arc radius of groove outline
R3	radius of groove fillet

https://doi.org/10.1017/aer.2021.1 Published online by Cambridge University Press

R^2	R-Squard
R_ε	strain ratio
RMSE	Root Mean Square Error
RMAE	Relative Maximum Absolute Error
RAAE	Relative Average Absolute Error
$S_{x_i'}$	model coefficient
Sf′	fatigue strength coefficient
Theta	gradient angle of the grooved web
u_i	upper limit on the dimension
UTS	Ultimate Tensile Strength
X	Latin hypercube matrix
X_{iu}	lower ranges of the variables
X_{il}	upper ranges of the variables
y_i	true value of test point responses
$\tilde{y}_i$	approximate value of test point responses
$\bar{y}$	mean value of test point responses
YS	yield strength
x	design variable vector
x_i	vector of the design variable

1.0 INTRODUCTION

To realise short-distance and instantaneous takeoff, carrier-based UAVs always utilise catapult takeoff as its takeoff method, but consequently, the drawbar suffers great tensile loads, which will reduce its life cycles and eventually lead to takeoff failure. In order to overcome this problem, the fatigue characteristic should be considered in the initial structure design.

The optimisation of the structure subjected to fatigue is of vital importance for aircraft landing system design, especially those with complex geometry characteristics and suffering severe working conditions. Formerly long computational times are also a barrier to these optimisation problems involved with many structural parameters. To save time, most traditional optimisation methodologies focus on the structures' static or quasi-static response or frequency response. However, modern computer development makes it possible using optimisation strategy based on fatigue analysis.

C. S. Johnson[(1)] put forward a computational framework for the optimisation of various aspects of rotor blades and applied metamodels and genetic algorithms to the model. Haiba et al.[(2)] introduced a life optimisation method to a suspension system of the vehicle. Meng et al.[(3)] used a surrogate model to solve a turbine blade design problem based on structural reliability analysis and uncertainties-based collaborative design. Xue et al.[(4)] improved particle swarm optimisation algorithm to take a lightweight design in a nose landing gear forward strut considering its fatigue life based on S-N analysis. Munk et al.[(5)] applied topology optimisation to aerospace design problems and designed a light aircraft landing gear. Xia et al.[(6)] applied DOE (design of experiments) and Kriging model in the optimisation to minimise the weight of the bolted connection of a wing bar, and specimen fatigue tests were carried out to evaluate the optimisation process.

https://doi.org/10.1017/aer.2021.1 Published online by Cambridge University Press

Although previous studies have solved problems in their corresponding fields, the structure optimisation method involving multi-parameter ejection structures is still a challenge to engineers concerned. For structures containing complex features, how to carry out structural and finite element parametric modeling, and build a joint optimisation platform for strain fatigue analysis remain a challenge for engineers. Moreover, parameters extraction, design of experiments, approximate model definition, and multi-parameter optimisation are also barriers to theoretical analysis and application research of each module. A joint simulation platform is established to achieve this goal, which combines parametric geometry modeling and finite element modeling, fatigue analysis, and parameters optimisation. By using this platform, a parametric drawbar model is built in 3D and discrete FEM model. Also, fatigue analysis based on lab tests and simulation is carried out for the validation of the model. Furthermore, a complete optimisation framework is built to obtain the optimum solution to improve the load-bearing and life of the drawbar.

This study is organised as follows. The lab fatigue test is carried out in Section 2, the numerical fatigue analysis and simulation model is also introduced, which can be verified by the test data. In Section 3, the geometry and FEM parametric model of the drawbar is built and the DOE method is introduced to select the most sensitive parameters for further optimization. In Section 2, sensitivity analysis is carried out to narrow the range of the parameters. In Section 5, a joint simulation platform is established to obtain an improving structure, during which process, a surrogate model is firstly provided to approximate the fatigue analysis in the given range, and then a global optimization algorithm is utilised.

The drawbar of a carrier-based aircraft suffers great overload during takeoff. Consequently, extreme tensile load acts instantaneously on the drawbar. This severe situation puts forward a great test on its bearing capacity and durability. The drawbar is manufactured based on traditional design criteria in structural strength without considering its fatigue life. As a result, in actual use, the drawbar is frequently confronted with a fatigue failure.

Due to the traditional design criteria' fault, a parameter optimisation based on the fatigue life is proposed to improve the load-bearing and life repeats of the drawbar.

2.0 FATIGUE LIFE EXPERIMENT AND NUMERICAL ANALYSIS OF A CARRIER-BASED AIRCRAFT DRAWBAR

2.1 Laboratory fatigue test of the drawbar

Laboratory fatigue test of the drawbar is carried out to examine the durability of the structure and test whether the structural fatigue life can meet the service requirements and improve the design, optimising the structure and prolonging service life.

Before structure experiments, the material basic mechanical properties are measured. Figure 1 shows the true stress-strain curve of the high-strength steel, which is obtained through variation from the nominal stress-strain relationship.

The drawbar suffers a shocking load during taking off. Figure 2 presents the load history. It can also be illustrated that the R ratio is zero in the fatigue test.

Then a laboratory test is carried out, the fracture is found on the head drawbar in the lab experiment, and the rest tests of the fatigue experiment are found the failure in the same region during 2,575 life repeats on average.

https://doi.org/10.1017/aer.2021.1 Published online by Cambridge University Press

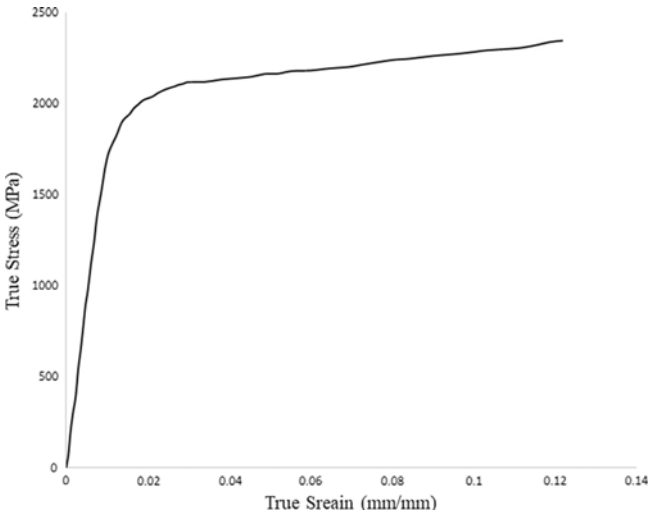

Figure 1. The true strain-stress curve of high-strength steel under tensile load.

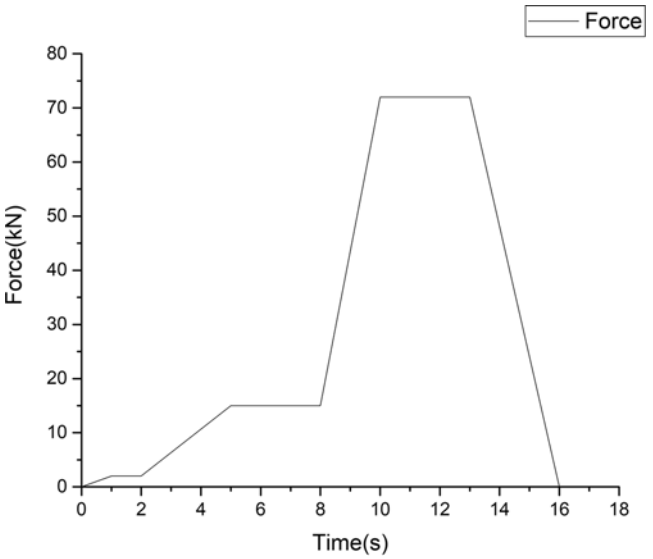

Figure 2. Load history of the drawbar.

The crack initiates from the groove root of the drawbar, then spreads upward to form a fracture and ultimately causes a fracture failure. Through the analysis of the fracture of the drawbar, and the life repeats reveal that failure belongs to the strain fatigue category.

2.2 Laboratory test results compared with simulation

FEM analysis software HyperMesh is used to simulate the stress feedback in the process of drawbar under tensile load. The FEM model is established as shown in the picture, meshing by Tetra10, with an amount of 94,572 elements in the size of 3 mm. The load direction is

https://doi.org/10.1017/aer.2021.1 Published online by Cambridge University Press

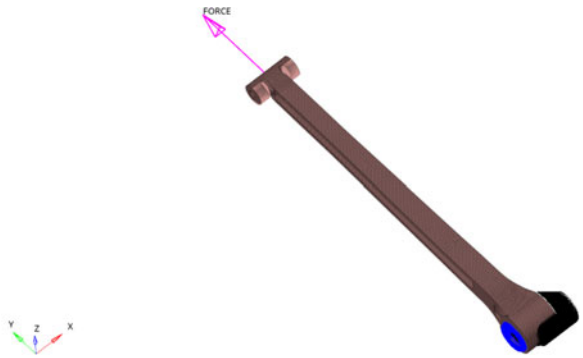

Figure 3. FEM model of the drawbar.

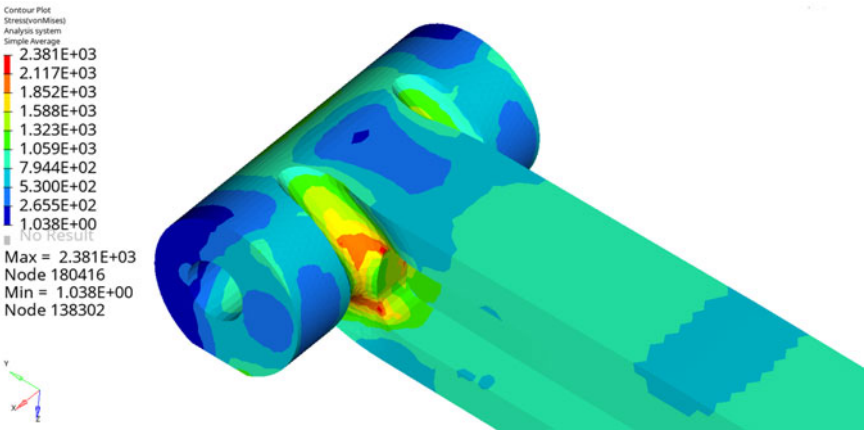

Figure 4. Stress contour plot.

along the drawbar axis. All degrees of freedom at the end of the drawbar are restrained except the degree of freedom around the axis of the hole. It can be seen from Fig. 3, all nodes degrees except Rotation-X are constrained.

A general implicit algorithm is utilised under statistic load conditions, Von-Mises stress contour plot (Fig. 4) shows good coincidence with the result of lab experiments drawn from the figure of comparison.

A static loading test of the drawbar is carried out. As the structure and its working condition is axial-symmetry, this study takes the mean value of the symmetrical strain gauge and compares simulation with test results. Figure 5 presents the positions of strain gauges. Table 1 shows the comparison between the maximum strain results measured by strain gauge and simulation results.

The good coincidence verifies the accuracy of the FEM model. From the contour plot, it can be seen that the maximum stress is 2,379MPa, located in the same position as the fracture is, which also exceeds the material high-strength steel's yield strength. It can be concluded that the area has stepped into the plastic zone of the structure.

https://doi.org/10.1017/aer.2021.1 Published online by Cambridge University Press

Table 1
Comparison of strain values

No.	Strain (με)	Simulation	Error
C1	2,196	2,227	1.41%
C2	2,207	2,248	1.86%
C3	3,593.5	3,560	0.93%
C4	3,960	3,940	0.51%
C5	3,501	3,525	0.69%
C6	3,930.5	3,925	0.14%
C7	3,489	3,592	2.95%
C8	4,051.5	3,992	1.47%
C9	3,278.5	3,264	0.44%
C10	3,967	3,853	2.87%
C11	3,755	3,740	0.40%
C12	3,724	3,730	0.16%
C13	3,843.5	3,838	0.14%
C14	3,752	3,738	0.37%
C15	3,949.5	4,010	1.53%
C16	3,710.5	3,790	2.14%
C17	2,810	2,781	1.03%
C18	2,849	2,797	1.83%

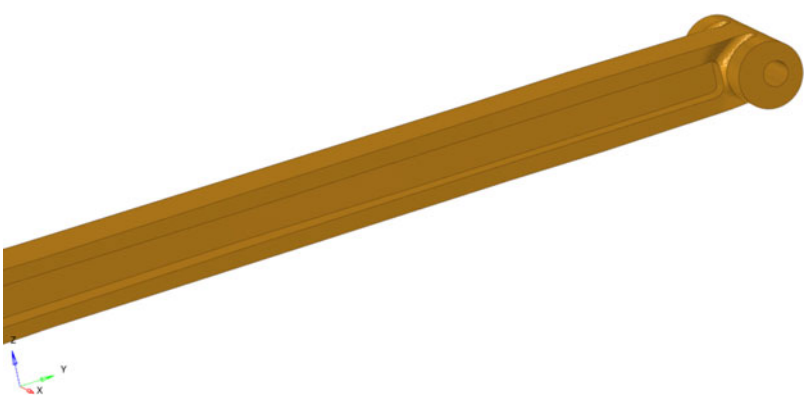

Figure 5. Positions of strain gauges.

2.3 Fatigue life analysis of drawbar

Deductions can be made that there appears strain fatigue, inferred from the smooth fracture surface, and 2,575 life repeats in the lab tests of this drawbar. This study applies the Coffin-Manson empirical formula to assess the life of the drawbar on the level of numerical theory. Of all $\Delta\varepsilon - N$ formulas, the Coffin-Manson formula is mostly used. The expression is defined as the following:

$$\varepsilon_{\mathrm{a}} = \varepsilon_{\mathrm{ea}} + \varepsilon_{\mathrm{pa}} = \frac{\sigma_f'}{E}(2N)^b + \varepsilon_f'(2N)^c. \quad \ldots(1)$$

https://doi.org/10.1017/aer.2021.1 Published online by Cambridge University Press

Table 2
Material fatigue parameter

Property	High-strength steel	Description
E	1.96E+05	Elastic Modulus (MPa)
ε_f'	0.133452	Fatigue Ductility Coefficient
K′	3,184.5	Cyclic Strength Coefficient (MPa)
Nc	2.00E+08	Cut-off
σ_f'	2,895	Fatigue Strength Coefficient (MPa)
UTS	1,930	Ultimate Tensile Strength (MPa)
YS	1,620	Yield Strength (MPa)
b	−0.087	Fatigue Strength Exponent
c	−0.58	Fatigue Ductility Exponent
me	0.3	Elastic Poisson's Ratio
mp	0.5	Plastic Poisson's Ratio
n′	0.15	Cyclic Strain Hardening Exponent

σ_f' defines the fatigue strength coefficient, ε_f' is coefficient for fatigue ductility, b is fatigue strength exponent, and c is the exponent for fatigue ductility. This formula reveals the relations between life N and elastic strain part ε_{ea}, plastic strain part ε_{pa} and the total ε_a.

The Coffin-Manson formula is used in structures of short or medium life repeats. When $R_\varepsilon \neq -1$, average stress should be corrected, and this model also needs correction. In this study, morrow total strain correction is introduced:

$$\varepsilon_a = \frac{\sigma_f' - \sigma_m}{\sigma_f'} \left[\frac{\sigma_f'}{E} (2N)^b + \varepsilon_f' (2N)^c \right] \quad \ldots (2)$$

where σ_m is the mean stress of the structure.

This study uses the fatigue analysis software nCode with its EN-CAE Fatigue module[7], and the material parameters are entered as Table 2 shows. The low-cycle fatigue performance parameters of metal materials under uniform temperature and axial constant amplitude strain control are determined according to ISO 1099-2017 Metallic Materials—Fatigue Testing—Axial Force-controlled Method.

Additionally, the E-N curve and elastoplastic boundary diagram of high-strength steel are drawn, and Fig. 6 shows the strain life with elastic and plastic lines.

Based on the work above, strain fatigue theory is used to calculate life repeats of the drawbar, of which life contour plot is shown as follows.

Figure 7 shows the life (repeats) contour plot, and the lowest life repeats' region appears at node 183,862 with 3,791 repeats. Figure 8 gives the precise location of the minimum life repeats.

Compared with lab experiments, simulation results show a precise coincidence in the fracture region and life repeats. Accordingly, the Coffin-Manson criterion is applied in subsequent analysis. Due to the conservative prediction in life calculation, results estimating from the Coffin-Manson criterion are higher than that testing in the lab.

https://doi.org/10.1017/aer.2021.1 Published online by Cambridge University Press

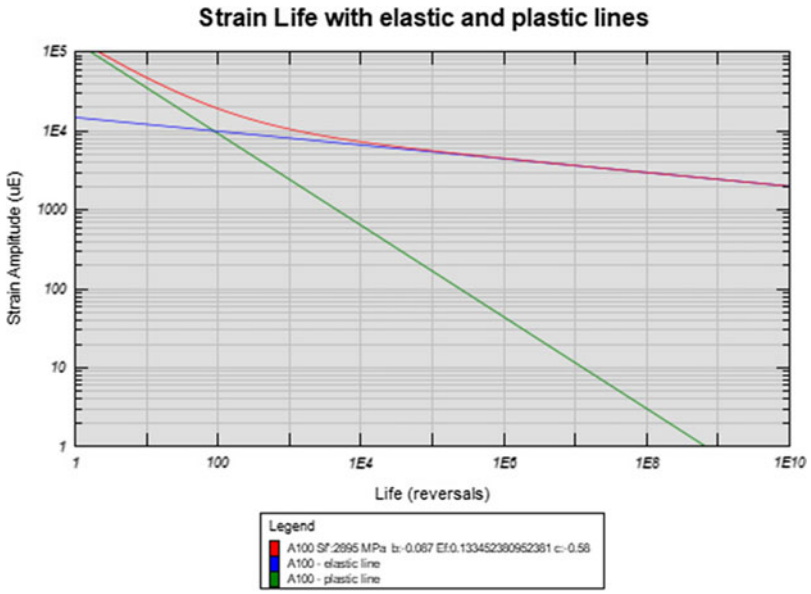

Figure 6. E-N curve and elastoplastic boundary of high-strength steel.

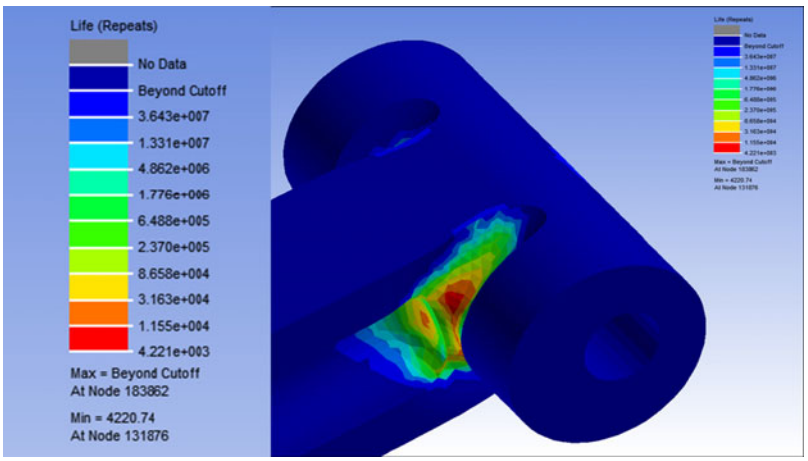

Figure 7. Life contour plot.

3.0 SURROGATE MODEL FOR FATIGUE LIFE

3.1 Parameters selection

Considering the structure's practical use, the manufacturing parameters are selected, and major structural parameters of the drawbar influencing its fatigue life and stress are illustrated as follows:

https://doi.org/10.1017/aer.2021.1 Published online by Cambridge University Press

Table 3
Range of drawbar parameters

Parameter	Lower bound	Upper bound
Beta	β	β+10
Theta	θ	θ+2.2
R_1	r_1	r_1+5
R_2	r_2	r_2+10
R_3	r_3	r_3+13
D_1	d_1	d_1+10
D_2	d_2	d_2+10
D_3	d_3	d_3+7
D_4	d_4	d_4+7
D_5	d_5	d_5+10
D_6	d_6	d_6+10
D_7	d_7	d_7+35
D_8	d_8	d_8+5

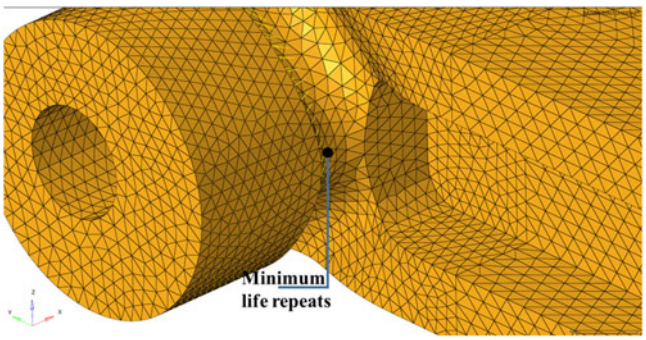

Figure 8. The node of minimum life repeats.

Beta: cutting edge angle of slotted feed knife
Theta: gradient angle of the grooved web
R_1: cutting edge radius of groove outline
R_2: arc radius of groove outline
R_3: radius of groove fillet
D_1: the distance between the axis of the drawbar body and center of groove outline cutter
D_2: the distance between the axis of drawbar head and center of groove outline cutter
D_3: the distance between the axis of the drawbar head and groove outline
D_4: the distance between the axis of the drawbar head and center of groove edge
D_5: height of groove
D_6: the distance between the axis of the drawbar head and gradient starting point
D_7: the distance between the axis of the drawbar head and gradient ending point
D_8: the initial thickness of web;

Figure 9 defines the 14 parameters of the drawbar in detail.

Initial ranges are also proposed on the basis of the drawbar geometry structural limits. On this basis, Table 3 roughly gives the range of the drawbar parameters.

https://doi.org/10.1017/aer.2021.1 Published online by Cambridge University Press

3.2 Establishment of the surrogate model

When a definite functional relationship cannot express the functional relationship between the objective function and the variables, it can be fitted by using the approximation models based on the data of sample points. And then, the optimal process can be carried out on this basis, which can significantly improve the efficiency when the variable space is large.

Surrogate model methods are based on the decomposition of $Y(x) = f(x) + \varepsilon(x)$, where the error $\varepsilon(x)$ is assumed to be identical independent distribution (normal distribution), $\varepsilon(x) \sim N(0, \sigma^2)$ for example. The process of creating surrogate models includes:

(i) Acquiring sample data given by DOE test design
(ii) Choosing the surrogate model type
(iii) Initializing the surrogate model
(iv) Verifying the surrogate model and the prediction effect by calculating the approximate error of the model

If the reliability is not high enough, the surrogate model needs to be updated to improve its prediction accuracy. The standard method is to add more sample data and change model parameters.

If the surrogate model has enough credibility, the simulation program can be replaced by the surrogate model;

Figure 10 shows the flow chart of the surrogate model.

The commonly used surrogate models include the response surface model, neural network model, orthogonal polynomial model, and Kriging model. The radial basis function neural network model (RBF)[8] is chosen in this model. Its advantages lie in its strong ability to approximate complex non-linear functions in engineering applications, no need for mathematical assumptions and black box characteristics. It has a strong fault-tolerant function. Even with noisy input, a sound network overall performance can be achieved.

The classical form of the radial basis function model can be expressed as follows[9].

$$f(x) = \sum_{i=1}^{n} \lambda_i \phi\left(\|x - x_i\|\right) \quad \ldots (3)$$

where n is the number of the sample points, x is the design variable vector, x_i is the vector of the design variable at the ith sample point, ϕ is a basis function, and λ_i is the coefficient of the ith basis function. The commonly used basis functions are shown as follows.

$$\text{Linear: } \phi(r) = r \quad \ldots (4)$$

$$\text{Gauss: } \phi(r) = e^{-cr^2}, \quad (0 < c < 1) \quad \ldots (5)$$

$$\text{Multiquadric: } \phi(r) = \sqrt{r^2 + c^2}, \quad (0 < c < 1) \quad \ldots (6)$$

R-Squard (R^2) is often used to measure the degree of consistency between the surrogate model and sample points.

$$R^2 = 1 - \frac{\sum_{i=1}^{n} (y_i - \tilde{y}_i)^2}{\sum_{i=1}^{n} (y_i - \bar{y})^2} \quad \ldots (7)$$

https://doi.org/10.1017/aer.2021.1 Published online by Cambridge University Press

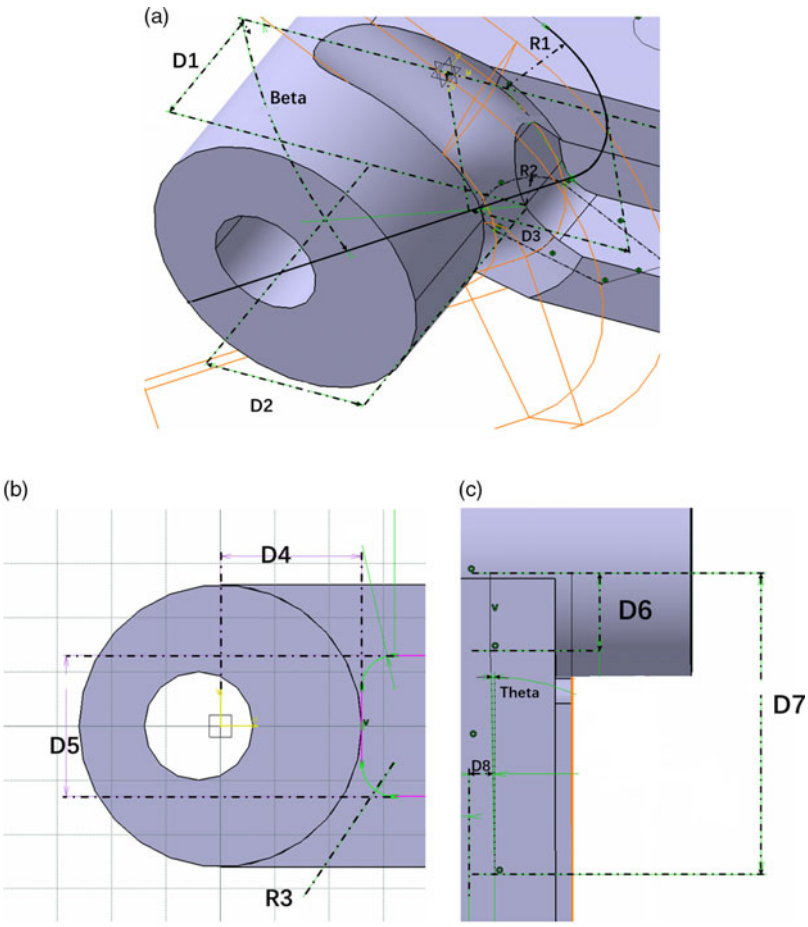

Figure 9. Major parameters of the drawbar.

where y_i, $\tilde{y}_i$, $\bar{y}$ represent the true values, approximate values and mean values of test point responses. The closer the value of $R^2$to 1, the higher the reliability of the approximation model will be. During the process, the initial number of sample points is 50; to get the best approximation content, 100 more points are added. Error analysis of the approximation model and other approximation models were also used. Figure 11 compares the R^2 values of different approximation models.

As is shown above, the RBF model has the highest reliability. To comprehensively evaluate the approximation of the model, Root Mean Square Error (RMSE), Relative Average Absolute Error (RAAE) and Relative Maximum Absolute Error (RMAE) are also introduced in this study[10].

$$RMSE = \sqrt{\frac{1}{n}\sum_{i=1}^{n}\left(y_i - \hat{y}_i\right)^2} \quad \ldots(8)$$

$$RAAE = \frac{\sum_{i=1}^{n}|y_i - \tilde{y}_i|}{n_t \times STD} \quad \ldots(9)$$

https://doi.org/10.1017/aer.2021.1 Published online by Cambridge University Press

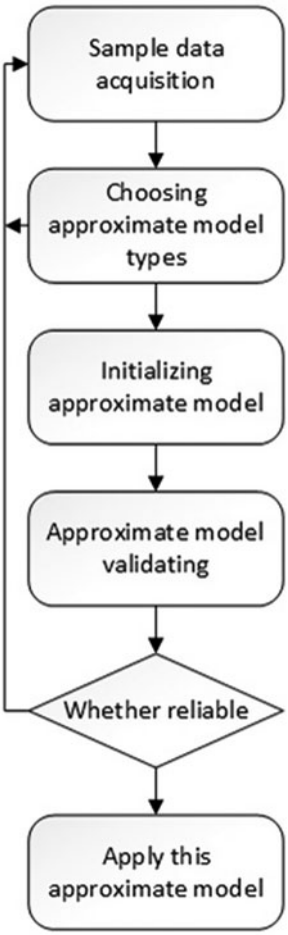

Figure 10. Process of establishing surrogate models.

$$STD = \sqrt{\frac{1}{n_t - 1}\sum_{i=1}^{n_t} y_i - \tilde{y}_i} \quad \ldots (10)$$

$$RMAE = \frac{\max(|y_1 - \tilde{y}_1|, |y_2 - \tilde{y}_2|, \cdots, |y_n - \tilde{y}_n|)}{STD} \quad \ldots (11)$$

The above four equations evaluate the accuracy of the surrogate model from different perspectives, R^2, RMSE, RAAE focus on describing the overall accuracy of the model, while RMAE on the local. Table 4 shows the confidence criterion of the model, which are given by the approximation module of the ISIGHT software[11].

The previous analysis indicates that the fitting relationship between sample optimisation objectives and variables can be accurately described by using the RBF model to fit the surrogate model.

https://doi.org/10.1017/aer.2021.1 Published online by Cambridge University Press

Table 4
Confidence criterion

Index	R^2	*RMSE*	*RAAE*	*RMAE*
Criterions	>0.9	<0.2	<0.2	<0.3
Values	0.9125	0.056	0.045	0.138

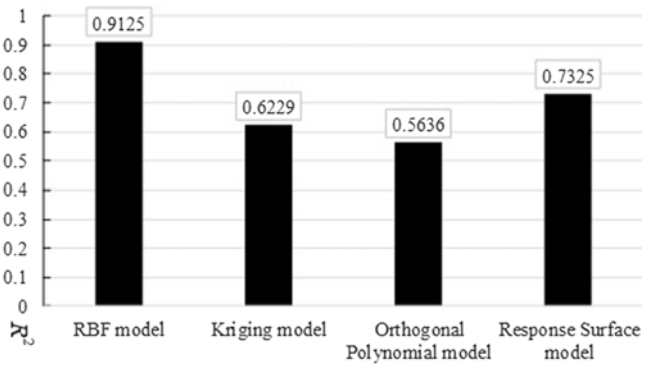

Figure 11. R^2 values of different approximation models.

3.3 Sensitivity analysis of drawbar parameters

Parameters affecting drawbar structure also have different influences on their static and fatigue responses, their ranges matter as well. We usually call this process sensitivity analysis. Performing sensitivity analysis can efficiently evaluate the influences of parameter varieties on structure response.

After the calculation of each sample point, the regression model is established according to the sample point. Through the Pareto chart, the relationship between each input variable and the maximum stress is analysed, as well as the information of correlation degree between variables and response. The positive effect or negative effect of each parameter on the response is also obtained. It is helpful to grasp the main parameters accurately in the design process.

Pareto chart, which is used to reflect the contribution of each input variable to each response, represents the main effect of all input variables in a given response, where blue represents the positive effect and red represents the negative effect. The value $N_{x_i'}$ is the percentage form of the model coefficient $S_{x_i'}$ after normalising the input variable.

$$N_{x_i'} = \frac{S_{x_i'}}{\sum_j \left| S_{x_i'} \right|} \times 100\% \qquad \ldots (12)$$

Figure 12 shows the Pareto chart of the analysis, and the values illustrate the positive/negative effects of each parameter. It can be illustrated from the Pareto chart that the variables D_4, R_3 have more positive effects, while the variables D_5, D_6 have more negative effects.

https://doi.org/10.1017/aer.2021.1 Published online by Cambridge University Press

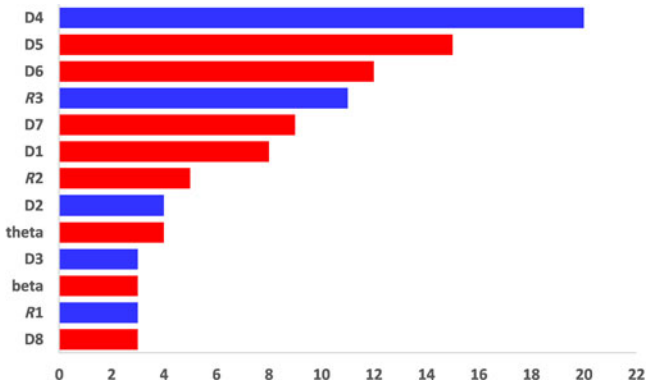

Figure 12. Pareto chart of the 13 variables.

4.0 OPTIMUM DESIGN OF STRUCTURAL PARAMETERS OF DRAWBAR

4.1 Design of experiments (DOE)

DOE is a branch of mathematical statistics and one of the most important statistical methods in product development and process optimization. Including:

- Identifying key experimental factors
- Determining the best combination of parameters
- Analyzing the relationship between input and output parameters and the trend of them
- Constructing empirical formulas and surrogate models
- Improving the robustness of design

This study builds a DOE platform, Fig. 13 shows the platform of drawbar optimisation simulation.DOE application includes a test plan, execution test and result analysis. There exist many methods to extract sample points, such as a full factorial design, orthogonal design, central composite design, uniform design, random design, Latin hypercube design and so on.

The Latin hypercube sampling (LHS) method is a widely used computer simulation design, which was first proposed by Mckay et al.[12]. It is a modified Monte Carlo method. The sample points are uniformly covered, which are more suitable for the case of more design variables. It can significantly reduce the scale of the experiment. Assuming the dimension of the design space is d, the number of sample points is n, and the range of coordinate points on a certain dimension is $x_i \in [l_i, u_i](i = 1, 2 \cdots, d)$, l_i represents the lower limit on this dimension, u_i is the upper limit:

(1) Determining the size of sampling n.
(2) Dividing the value range of each dimension variable x_i into n intervals, then the design space will be divided into n^d sub-regions.
(3) Randomly producing a matrix of $n \times d$, each column of which is a full random permutation, matrix $\mathbf{X}$ is called Latin hypercube matrix.
(4) Each row of matrix $\mathbf{X}$ corresponds to a selected small hypercube. A sample point can be obtained by randomly extracting a sample point in this region, n sample points can be obtained.

https://doi.org/10.1017/aer.2021.1 Published online by Cambridge University Press

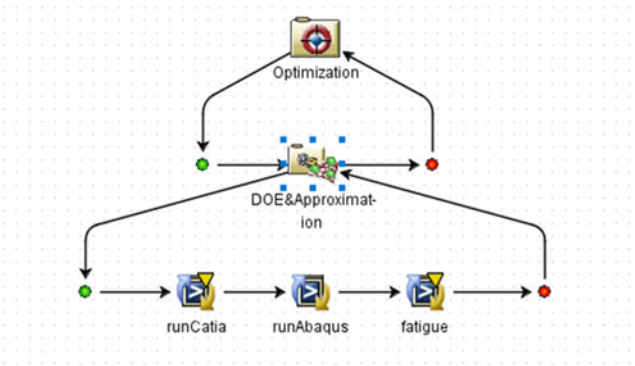

Figure 13. DOE platform of a drawbar joint simulation.

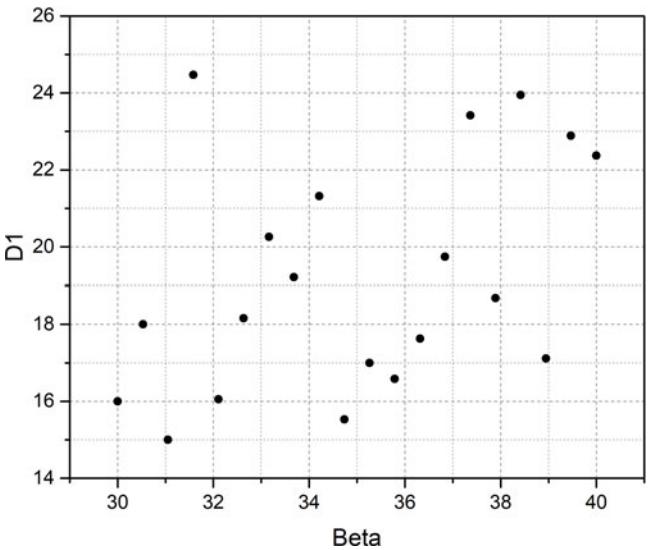

Figure 14. Distribution of sample points using LHS.

The following figure shows the distribution of sample points selected by LHS.

Compared with the original Latin hypercube method given in Fig. 14, the uniformity of the 20 sample points of *Beta* versus D_1 in two-dimensional space obtained by the improved hypercube sample design[13] method is obviously improved as Fig. 15 presents.

3.2 Optimum design of the drawbar based on MIGA

The optimisation problems in aircraft design and manufacturing engineering are often complex. The objective functions are multimodal, non-linear, discontinuous and non-differentiable. The design variables and constraint functions may also be linear, non-linear, continuous or discrete sets of variables. Traditional gradient optimization and direct search often fail to find the global optimal solution. On the basis of this cognition, global optimisation is used in this study.

https://doi.org/10.1017/aer.2021.1 Published online by Cambridge University Press

Table 5
MIGA parameters

Parameter	Value
Sub-population size	10
Number of islands	20
Number of generations	20
Rate of crossover	0.8
Rate of mutation	0.01
Rate of migration	0.3
Interval of migration	5
Relative tournament size	1
Elite size	0.5

Table 6
Optimised drawbar parameters

Parameter	Value
Beta	$\beta + 9.7$
Theta	$\theta + 0.5$
R_1	r_1+1.6
R_2	r_2+5.8
R_3	r_3+1
D_1	d_1+4.4
D_2	d_2+5.6
D_3	d_3+4
D_4	d_4+1
D_5	d_5+3
D_6	d_6+4.5
D_7	d_7+21
D_8	d_8+8

Global optimisation algorithms[14] include multi-island genetic algorithm, pointer automatic optimiser, evolutionary optimisation, adaptive simulated annealing and particle swarm optimisation.

In this paper, a multi-island genetic algorithm is used to optimise the drawbar. The parameters concerned in MIGA is listed in Table 5.

Range of the geometry is the same as those defined in DOE, and the numerical expression of the optimisation process is defined as the following:

$$\begin{cases} max \quad L(X_i) \\ \text{s.t.} \quad X_{il} \le X_i \le X_{iu} \end{cases} \qquad \ldots (13)$$

The parameters above are optimised and the global search is carried out to reduce the maximum stress. The final results are shown in Table 6:

https://doi.org/10.1017/aer.2021.1 Published online by Cambridge University Press

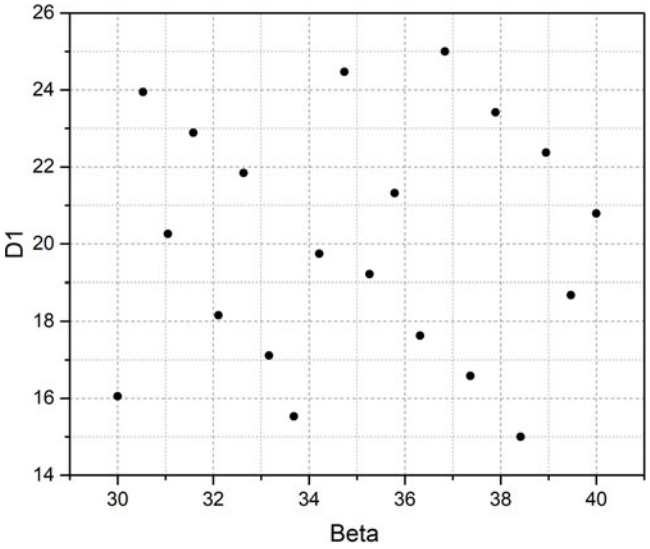

Figure 15. Distribution of sample points using improved LHS.

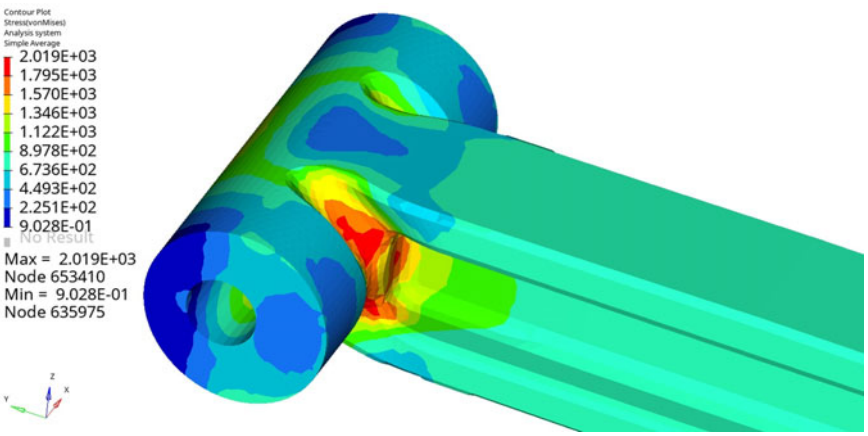

Figure 16. Stress contour plot of the optimised drawbar.

The optimised results are modeled and analysed by FEM. The stress and strain contour plots are shown in Fig. 16.

The maximum stress value is 2,010MPa in the same position as before. Compared with 2,379MPa before optimisation, the stress level decreases by 373MPa, 15.7%. Compared with the results optimised by the multi-island genetic algorithm, the stress error is 0.74%.

Importing the stress calculation results into a fatigue analysis module for life simulation calculation, the final results are shown in Fig. 17.

The final fatigue life calculation results are 8,420 takeoffs and landings at node No. 653410, also with an error of 0.93% between optimisation results. Compared with that before optimisation, life repeats increase by 4,629,122%.

https://doi.org/10.1017/aer.2021.1 Published online by Cambridge University Press

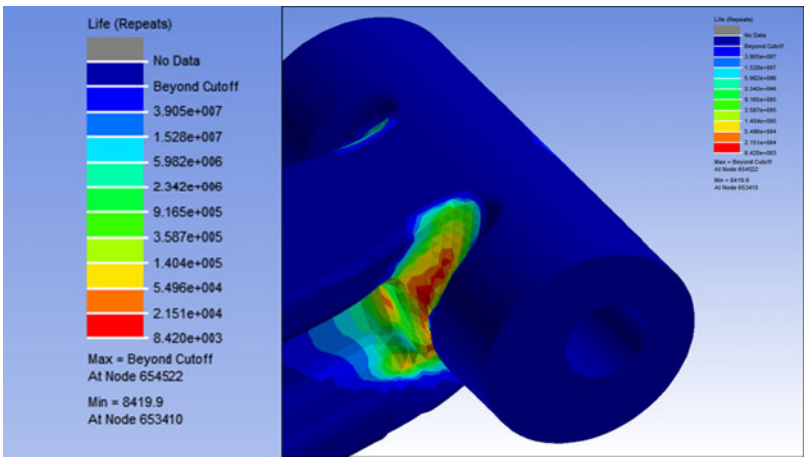

Figure 17. Life contour plot after optimization.

5.0 CONCLUSIONS

In this study, a new design strategy for carrier-based UAV drawbar is put forward and validated by a practical engineering application. The finite element simulation of the drawbar structure is carried out including life assessment. On the basis of the simulation, the parametric joint optimisation platform is established, and the following conclusions are obtained:

The fatigue life assessment method of the drawbar structure established in this paper is relatively reliable compared with the laboratory life test.

The surrogate model fitted by the sample points generated by the Latin hypercube method is of high reliability, which is up to 91%.

Thirteen parameters are optimised by a multi-island genetic algorithm, and the optimal solution is sought for 500 times of iteration. The maximum stress error between the fitted optimal solution and the modified finite element model is 0.74%, and the life repeats error is 0.93%.

After optimisation, in simulation results, the maximum stress of the drawbar has been decreased by 15.7% while the life calculation increased by 122%.

REFERENCES

1. JOHNSON, C. and BARAKOS, G. A framework for optimising aspects of rotor blades, *Aeronaut J (1968)*, 2011, **115**, (1165), pp 147–161. doi: 10.1017/S0001924000005558
2. HAIBA, M., BARTON, D.C., BROOKS, P.C. and LEVESLEY, M.C. The development of an optimization algorithm based on fatigue life, *Int J Fatigue*, 2003, **25**, (4), pp 299–310.
3. MENG, D., YANG, S., ZHANG, Y., & SHUN-PENG, Z. Structural reliability analysis and uncertainties-based collaborative design and optimization of turbine blades using surrogate model. *Fatigue & Fracture Eng. Mater. Struct.*, 2019, **42**, (6), pp 1219–1227.
4. XUE, C.J., DAI, J.H., WEI, T., *et al.* Structural optimization of a nose landing gear considering its fatigue life. *J Aircr*, 2012, **49**, (1), pp 225–236.
5. MUNK, D.J., AULD, D.J., STEVEN, G.P. and VIO, G.A. On the benefits of applying topology optimization to structural design of aircraft components. *Struct Multidiscipl Optim*, 2019, **60**, (3), pp 1245–1266.

https://doi.org/10.1017/aer.2021.1 Published online by Cambridge University Press

6. XIA, T., *et al.* Metamodel-based optimization of the bolted connection of a wing spar considering fatigue resistance. *Proc Inst Mech Eng G. J Aerosp Eng,* 2016, **230**, (5), pp 805–814. doi: 10.1177/0954410015598792.
7. HBM nCode: DesignLife Theory Guide. HBM United Kingdom Limited, 2015, Rotherham.
8. HARDY, R.L. Multiquadric equations of topography and other irregular surfaces, *J Geophy*, 1971, **76**, (8), pp 1905–1915.
9. FANG, H., and HORSTEMEYER, M. Metamodeling with Radial Basis Functions, 46th AIAA/ASME/ASCE/AHS/ASC Structures, Structural Dynamics and Materials Conference, Austin, TX, AIAA Paper 2005-2059, April 2005.
10. JIN, R., CHEN, W. and SIMPSON, T. Comparative studies of metamodelling techniques under multiple modelling criteria. *Struct Multidisc Optim*, 2001, **23**, pp 1–13. https://doi.org/10.1007/s00158-001-0160-4.
11. Simulia Isight: ISIGHT Users' Guide. Dassault Systems, 2016, Paris.
12. MCKAY, M.D., *et al.* A comparison of three methods for selecting values of input variables in the analysis of output from a computer code. *Technometrics*, 1979, **21**, (2), pp 239–245
13. FLORIAN, A. An efficient sampling scheme: updated Latin hypercube sampling. *Probabilistic Eng Mech*, 1992, **7**, (2), pp 123–130.
14. PAN, M.H., TANG, W.C., XING, Y. and NI, J. The clamping position optimization and deformation analysis for an antenna thin wall parts assembly with ASA, MIGA and PSO algorithm. *Int J Precis Eng Manuf*, 2017, 18, (3), pp 345–357.

https://doi.org/10.1017/aer.2021.1 Published online by Cambridge University Press